Nonlinear Dynamic Response of RC Buildings with Different Base-Isolation Systems Subjected to Near-Fault Earthquakes

F. Mazza, M. Mazza & A. Vulcano
Dipartimento di Strutture, Università della Calabria, Rende (Cosenza), Italy

15 WCEE
LISBOA 2012

SUMMARY:
Near-fault ground motions are characterized by long-duration horizontal pulses and high values of the peak vertical acceleration, which can become critical for a base-isolated structure. In order to check if current provisions of the Italian seismic code can be considered adequate for the design of base-isolated structures located in a near-fault area, base-isolated five-storey r.c. framed buildings with elastomeric bearings acting alone or combined in parallel or in series with sliding bearings are studied. The base-isolated structures are designed assuming the same values of the fundamental vibration period and equivalent viscous damping in the horizontal direction. The nonlinear analysis of the test structures subjected to horizontal and vertical components of near-fault ground motions is performed checking plastic conditions at the potential critical sections of the girders and columns. The response of an elastomeric bearing is simulated by a model with variable stiffness properties in the horizontal and vertical directions, depending on the axial force and lateral deformation, while a rigid-plastic (with friction variability) law is assumed to simulate the behaviour of a sliding bearing.

Keywords: base-isolated buildings, elastomeric and sliding bearings, near-fault motions, nonlinear dynamic analysis.

1. INTRODUCTION

Base-isolation of a structure subjected to an earthquake allows a considerable reduction of the horizontal loads transmitted to the superstructure by using deformable (e.g. HDLRBs) and/or frictional (e.g. steel-PTFE sliding bearings) devices. The following isolation strategies, or a suitable combination of them, can be used (Braga et al., 2005): increase of the fundamental vibration period of the structure, to shift it in the range of low spectral accelerations; limitation of the maximum force transmitted to the superstructure, as a function of the friction coefficient. In case of elastomeric bearings acting alone ("Base Isolation", BI, systems) or combined in series with sliding bearings ("Base Isolation and in-Series Sliding", BISS, systems), the structure behaves as isolated or fixed-base along the vertical direction depending on the value, respectively very low or very high, of the ratio $\alpha_{K0}(=K_{V0}/K_{H0})$ between the vertical (K_{V0}) and horizontal (K_{H0}) nominal stiffnesses of the isolation system. Moreover, a fixed-base structure is expected in the vertical direction for the Base Isolation with in-Parallel Sliding (BIPS) systems, also depending on the high stiffness of the grid of girders placed at the level of the isolation system. In this case, a fixed-base structure is obtained in the horizontal direction until the friction threshold imposed by the sliding bearings is not exceeded.

Near-fault ground motions are characterized by long-duration horizontal pulses and high values of the ratio α_{PGA} between the peak value of the vertical acceleration (PGA_V) and the analogous value of the horizontal acceleration (PGA_H), which can become critical for a base-isolated structure. More specifically, the horizontal deformability of a base-isolated structure may amplify the inelastic response of the superstructure and induce a failure of the isolation system (Mazza and Vulcano, 2009). Moreover, high values of α_{PGA} can notably modify the axial load in r.c. columns and the ductility demand along the span of the girders (Mazza and Vulcano, 2012), while elastomeric and sliding bearings can undergo tensile loads (Kasalanati and Constantinou, 2005) and uplifts (Ryan and Chopra, 2006), respectively. Different in-plan combinations and configurations of elastomeric and sliding bearings are compared in the present work, referring to base-isolated five-storey r.c. framed buildings located in a near-fault area and designed according to the Italian Technical Regulations for Constructions, 2008 (NTC08). The effectiveness of NTC08 rules is investigated considering the test structures subjected to horizontal and vertical near-fault ground motions.

2. MODELING OF THE BASE-ISOLATED R.C. FRAMED STRUCTURES

The base-isolation systems are generally realized by elastomeric and/or frictional bearings (e.g., Naeim and Kelly, 1999; Mazza and Vulcano, 2010), aiming to carry the vertical loads (exhibiting a rather high vertical stiffness) and to allow rather large horizontal displacements (exhibiting a low stiffness or strength in the horizontal direction). The large horizontal base displacement consequent to a near-fault ground motion can be enabled by oversizing the elastomeric bearings (e.g., increasing the geometric dimensions of the rubber layers) or increasing the roughness of the sliding surface of the frictional bearings. In alternative, the elastomeric bearing may act in parallel with a sliding bearing (e.g., the "Resilient-Friction Base Isolator", R-FBI) or in series with a sliding plate (e.g., the "Electricité de France" system, EDF) attached to its top or bottom surface. However, the Base Isolation with in-Parallel Sliding (BIPS) system can increase the contribution of the higher vibration modes of the superstructure, while the Base Isolation with in-Series Sliding (BISS) system is not always favourable in reducing the residual displacement of the isolation system. The behaviour of the above illustrated base-isolation systems can be simulated by adopting the models shown in Figure 1. More specifically, Figures 1a and 1b refer, respectively, to elastomeric and frictional bearings, while Figures 1c and 1d represent, respectively, BIPS and BISS systems.
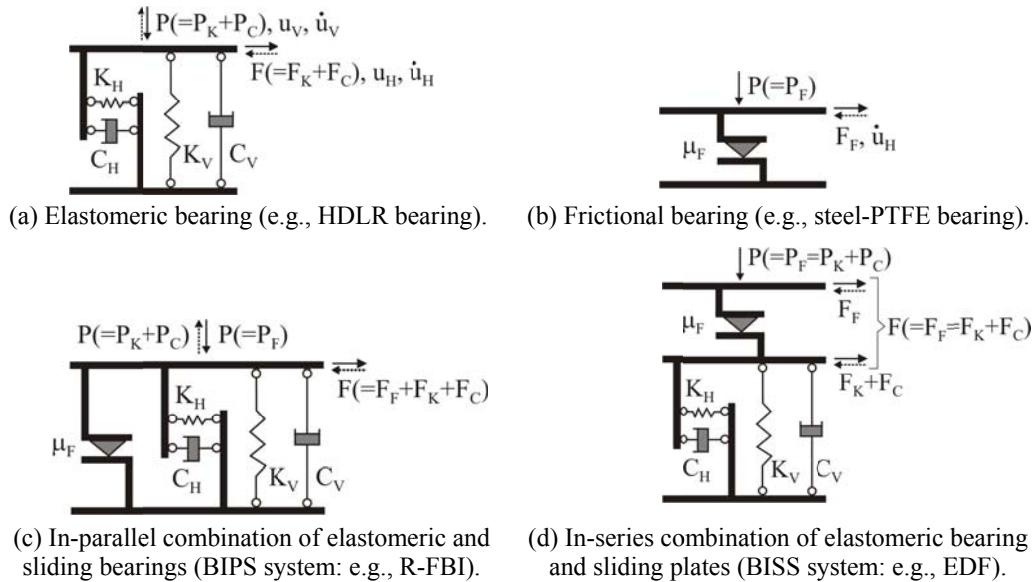

(a) Elastomeric bearing (e.g., HDLR bearing).   (b) Frictional bearing (e.g., steel-PTFE bearing).

(c) In-parallel combination of elastomeric and   (d) In-series combination of elastomeric bearing
    sliding bearings (BIPS system: e.g., R-FBI).   and sliding plates (BISS system: e.g., EDF).

Figure 1. Modeling of base-isolation systems.

Elastomeric bearings (e.g., the high-damping-laminated-rubber-bearings, HDLRBs) provide energy dissipation and re-centring capability. Experimental results by Ryan et al. (2004) pointed out that the horizontal stiffness of a HDLRB (starting from K_{H0}) decreases with increasing vertical load (P), while the corresponding vertical stiffness (starting from K_{V0}) decreases with increasing lateral deformation (u_H). To account for the observed behaviour, the two-spring-two-dashpot model shown in Figure 1a, constituted of nonlinear spring acting in parallel with a linear viscous dashpot both in the horizontal and vertical directions, can be adopted (Mazza and Vulcano, 2012). The nonlinear force-displacement laws for the horizontal (F_K-u_H) and vertical (P-u_V) springs are given as (Naeim and Kelly, 1999; Ryan et al., 2004)

$$F_K = K_H u_H = K_{H0}\left[1 - \left(P/P_{cr}\right)^2\right]u_H \quad , \quad P_K = K_V\left(u_V - \frac{\alpha_b}{\alpha_{K0}}\frac{16}{\pi^2 \phi_b S_2}u_H^2\right) \qquad (1a,b)$$

where the compressive or tensile critical load (P_{cr}) and the vertical stiffness (K_V) can be obtained according to experimental observations (Kelly, 2003; Ryan et al., 2004) and, after some manipulation, can be specialized for a circular bearing of diameter ϕ_b as

$$P_{cr} = \pm\left(\pi\phi_b/4\right)K_{H0}\sqrt{\alpha_{K0}} \qquad , \qquad K_V = K_{V0}\Big/\left[1 + 48\left(u_H/\pi\phi_b\right)^2\right] \qquad (2a,b)$$

where $\alpha_b = h_b/t_r$, h_b and t_r being the total height of the bearing and the thickness of the rubber, respectively (e.g., $\alpha_b = 1.2$ can be considered as a mean value); $S_2 = \phi_b/t_r$, the secondary shape factor (e.g., $S_2 \geq 4$ is a conservative assumption against buckling).

Moreover, the linear force-velocity laws for the horizontal (F_C - $\dot{u}_H$) and vertical (P_C - $\dot{u}_V$) dashpots in Figure 1a are expressed as

$$F_C = C_H \dot{u}_H \cong (\xi_H K_{H0} T_{1H}/\pi)\dot{u}_H \qquad , \qquad P_C = C_V \dot{u}_V \cong (\xi_V K_{V0} T_{1V}/\pi)\dot{u}_V \qquad (3a,b)$$

where ξ_H (ξ_V) and T_{1H} (T_{1V}) represent the equivalent viscous damping ratio and the fundamental vibration period in the horizontal (vertical) direction, respectively.

The response of a steel-PTFE sliding bearing (Figure 1b) basically depends on sliding velocity, contact pressure and temperature (e.g., Dolce et al., 2005). More specifically, the coefficient of sliding friction increases with increasing velocity up to a certain velocity value, beyond which it remains almost constant, while drops with increasing pressure (with a rate of reduction that is dependent on sliding velocity) and temperature. The frictional force at the sliding interface can be expressed as

$$F_F = \mu_F \cdot P \cdot Z \qquad , \qquad \mu_F = \mu_{max} - (\mu_{max} - \mu_{min}) \cdot e^{-\alpha \dot{u}_H} \qquad (4a,b)$$

where Z is a dimensionless hysteretic quantity (Z takes values of ± 1 during sliding and less then unity during sticking) and μ_F is the coefficient of friction at sliding velocity $\dot{u}_H$, which attains the value μ_{max} or μ_{min} respectively at high or very low velocity, while α is a constant for given values of pressure and temperature. The r.c. frame members are idealized by means of a two-component model, constituted of an elastic-plastic component and an elastic component, assuming a bilinear moment-curvature law. The effect of the axial load on the ultimate bending moment of the columns (M-N interaction) is also considered, assuming fully elastic both the axial and shear strains. At each step of the analysis, the elastic-plastic solution is evaluated in terms of the initial state and the incremental load on the basis of a holonomic law, as a solution of the Haar-Kàrmàn principle (Mazza and Vulcano, 2009). More specifically, by imposing plastic conditions on the bending moments (m_i and m_j) at the end sections (i and j) of each frame element, the elastic-plastic solution can be obtained considering, among the equilibrated internal forces $\mathbf{m}=(m_i, m_j)^T$, the one resulting closest to the elastic solution $\mathbf{m}_E=(m_{Ei}, m_{Ej})^T$ and satisfying the complementary energy minimum condition for the self-equilibrated internal forces ($\mathbf{m}-\mathbf{m}_E$). The above solution can be easily obtained by using the three-step algorithm illustrated in Figure 2, where M_{y1} (M_{y4}) and M_{y3} (M_{y2}) represent, respectively, the yield moments producing tension at top and bottom of the end section i (j).
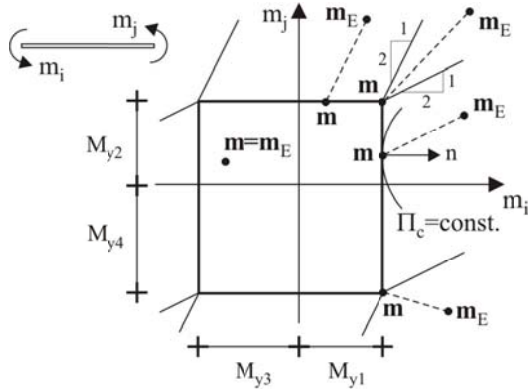
$$m_i' = \max\left\{-M_{y3}, \ \min\left\{M_{y1}, m_{Ei}\right\}\right\} \qquad (5a)$$

$$m_j = \max\left\{-M_{y4}, \ \min\left\{M_{y2}, m_{Ej} - \frac{1}{2}(m_{Ei} - m_i')\right\}\right\} \qquad (5b)$$

$$m_i = \max\left\{-M_{y3}, \ \min\left\{M_{y1}, m_{Ei} - \frac{1}{2}(m_{Ej} - m_j)\right\}\right\} \qquad (5c)$$

Figure 2. Elastic-plastic solution of a r.c. frame member according to the Haar-Kàrmàn principle.

3. DESIGN OF THE BASE-ISOLATED R.C. FRAMED STRUCTURES

A typical five-storey residential building, with r.c. framed structure isolated at the base by different systems (Figure 3), is considered as a reference for the numerical investigation. Because of the structural symmetry and assuming the floor slabs infinitely rigid in their own plane, the entire structure is idealized by an equivalent plane frame along the horizontal motion direction (Figure 3b), whose elements have stiffness and strength properties so that the two lateral frames, the two interior frames and the central one could be represented as a whole. The tributary mass resulting from the overall building and the gravity loads corresponding to the tributary area marked in Figure 3a are considered for each of them, assuming infilled walls placed along the perimeter of the building as non-structural elements regularly distributed in elevation. Length and cross-sections of the frame members are also shown in Figure 3. Specifically, different in-plan combinations and configurations of elastomeric and sliding bearings are considered: elastomeric bearings

(i.e. BI configuration in Figure 4a: HDLRBs type 1, which are assumed with the same dimensions for the sake of simplicity and in order to reduce torsional effects); in-parallel combinations of elastomeric and sliding bearings (i.e. BIPS-A, BIPS-B and BIPS-C configurations in Figures 4b, 4c and 4d, respectively: HDLRBs type 2); in-series combinations of elastomeric and sliding bearings (i.e. BISS-A, BISS-B and BISS-C configurations in Figures 4e, 4f and 4g, respectively: HDLRBs type 3, with sliding bearings in the same position adopted for the BIPS systems but placed in-series with HDLRBs type 1). Each arrangement of elastomeric and sliding bearings corresponds to a value of the nominal sliding ratio $\alpha_{S0}(=F_{S0}/F_{S0,max})$, defined, under gravity loads, as the global sliding force (F_{S0}) corresponding to an examined BIPS (Figures 4b, 4c and 4d) or BISS (Figures 4e, 4f and 4g) system divided by the maximum sliding force ($F_{S0,max}$), this latter evaluated supposing that elastomeric and sliding bearings (or plates) are placed under each column. Three values of the nominal stiffness ratio of the HDLRBs (i.e. α_{K0}=200, 800, 2000) are considered for the BI, BIPS-A and BISS-A structures, while α_{K0}=800 is assumed for the BIPS-B, BIPS-C, BISS-B and BISS-C ones. The base-isolated structures are designed assuming the same values of the fundamental vibration period in the horizontal direction (i.e. T_{1H}=2.5 s) and equivalent viscous damping ratios in the horizontal (i.e. ξ_H=10%) and vertical (i.e. ξ_V=5%) directions. Moreover, the equivalent viscous damping of the sliding bearings (ξ_{HS}) is calculated referring to the (horizontal) spectral displacement, considering the gravity loads and a sliding friction coefficient μ_F=0.03. For each of the thirteen cases considered in the analysis, the following data are reported in Table 1: nominal values of the stiffness (α_{K0}) and sliding (α_{S0}) ratios; equivalent viscous damping of the elastomeric (ξ_{HI}) and sliding (ξ_{HS}) bearings, in the horizontal direction; diameter of the HDLRBs (ϕ_b) and corresponding primary (S_1) and secondary (S_2) shape factors; compression modulus of the rubber-steel composite bearing (E_c).

The proportioning of the test structures is done according to the Italian seismic code (NTC08) assuming, besides the gravity loads, the horizontal and vertical seismic loads with a same value of the behaviour factor (i.e. q_H=q_V=1.5). Moreover, the following design assumptions are made: moderately soft soil (class D, subsoil parameters: S_{SH}=1.45 in the horizontal direction and S_{SV}=1 in the vertical one); flat terrain (class T1, topographic parameter: S_T=1); high-risk seismic region (peak ground acceleration in the horizontal, PGA_H, and vertical, PGA_V, directions equal to 0.404g and 0.278g, respectively). The gravity loads used in the design are represented by dead- and live-loads, respectively equal to: 4.3 kN/m^2 and 1 kN/m^2, for the top floor; 5 kN/m^2 and 2 kN/m^2, for the other floors. The contribution of the masonry-infills is taken into account considering a weight of 2.7 kN/m^2. The following masses are considered at each floor: lumped masses at the exterior and interior joints, in order to take into account the contribution of the transverse girders and, in case of the exterior joints, also the one of the masonry infills; uniformly distributed mass along the girders and columns, accounting for the gravity load of the structural member and, in the case of a girder, also for that of the floor slab and masonry infills (only for girders of lateral frames). A cylindrical compressive strength of 25 N/mm^2 for concrete and a yield strength of 450 N/mm^2 for steel are assumed.
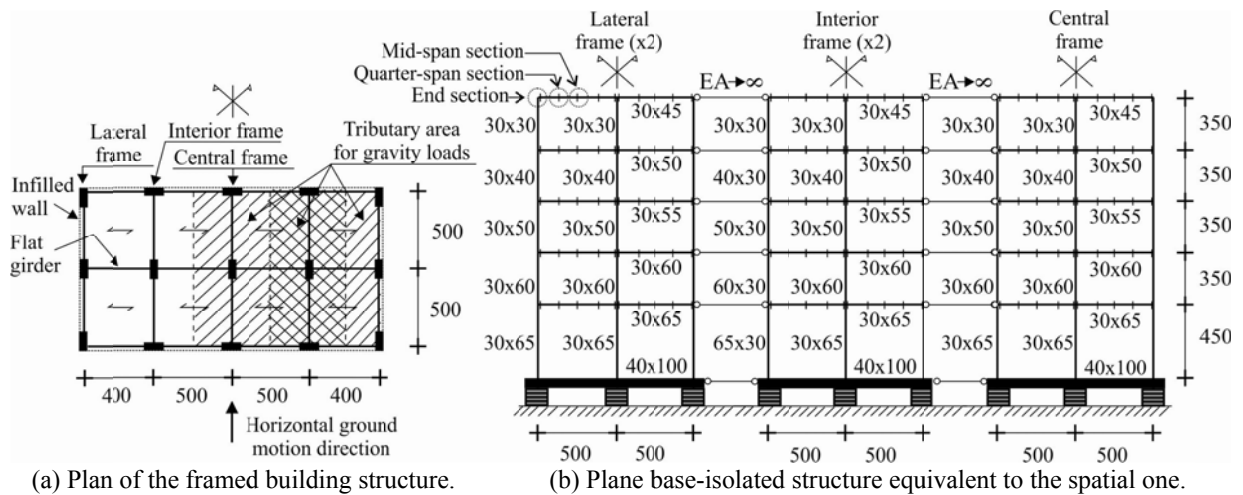

Figure 3. Reference base-isolated r.c. framed structure (dimensions in cm).

The design of the superstructure has been carried out satisfying minimum conditions for the longitudinal bars of the girders and columns, according to the provisions for low ductility class imposed by NTC08: at least two 14 mm bars are provided both at the top and bottom throughout the length of all the frame

members; for the girders, a tension reinforcement ratio not less than 0.31% (for the assumed yield strength) is provided and, at their end sections, a compression reinforcement not less than half of the tension reinforcement is placed; a minimum steel geometric ratio of 1% is assumed for the symmetrically-reinforced section of each column.
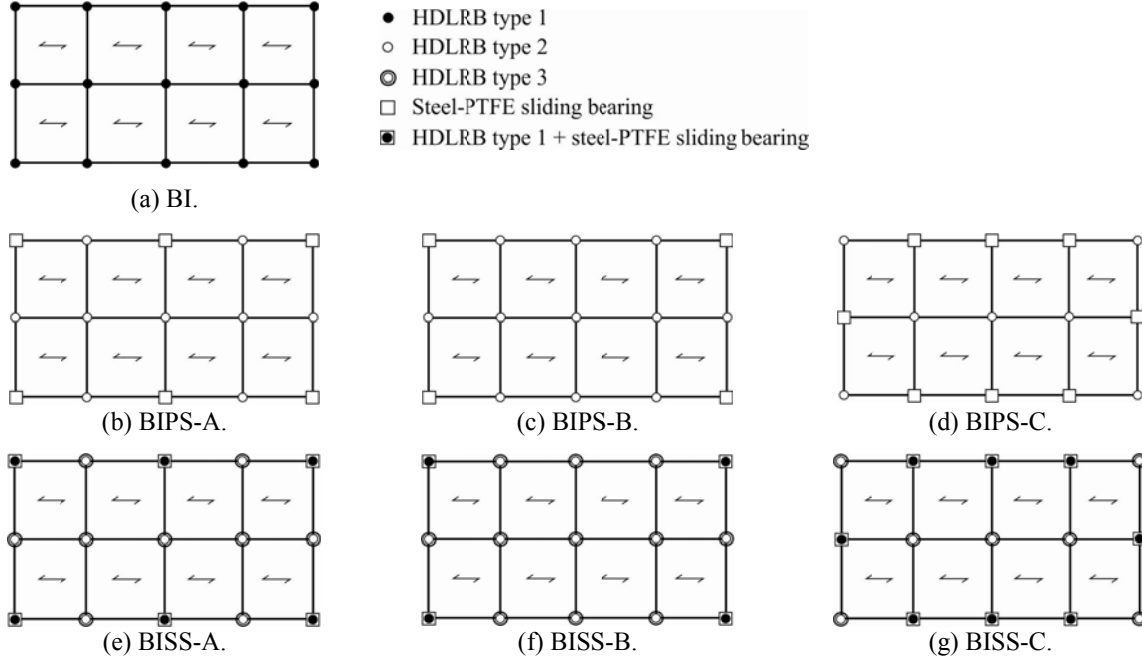

- HDLRB type 1
- HDLRB type 2
- HDLRB type 3
- Steel-PTFE sliding bearing
- HDLRB type 1 + steel-PTFE sliding bearing

(a) BI.

(b) BIPS-A.   (c) BIPS-B.   (d) BIPS-C.

(e) BISS-A.   (f) BISS-B.   (g) BISS-C.

Figure 4. In-plan layout of the base-isolation systems.

The design of the HDLRBs has been carried out according to the prescriptions imposed by NTC08, assuming a shear modulus of the elastomer G=0.35 MPa. In particular, the Ultimate Limit State (ULS) verifications regarding the maximum shear strains have been satisfied: i.e. $\gamma_{tot}=\gamma_s+\gamma_c+\gamma_\alpha\leq5$ and $\gamma_s\leq2$, where γ_{tot} represents the total design shear strain, while γ_s, γ_c and γ_α represent the shear strains of the elastomer due, respectively, to seismic displacement, axial compression and angular rotation. Moreover, the maximum compression axial load (P) is not exceeded the critical load (P_{cr}; see Equation 2a) divided by a safety coefficient equal to 2.0. Finally, the minimum tensile stress (σ_t) resulting from the seismic analysis has been assumed as 2G(=0.7 MPa) for all the elastomeric bearings. In Table 1 the results of the ULS verifications for the HDLRBs are also reported. As can be observed, the design of the HDLRBs has been controlled by the condition imposed on the maximum shear strains (i.e. γ_{tot} and γ_α), with some exceptions for BI (i.e. α_{K0}=200 and 800) and BISS-A (i.e. α_{K0}=200) structures where the buckling control proved to be the more restrictive. No tensile axial loads were found.

Table 1. Geometric and mechanical properties of the base-isolation systems.

Test structure	α_{K0}	α_{S0}	ξ_{HI} (%)	ξ_{HS} (%)	ϕ_b (cm)	S_1	S_2	E_c (MPa)	γ_s	γ_{tot}	P/P_{cr}
BI	200	-	10	-	107	5.61	2.20	63	0.48	2.15	0.50
	800	-	10	-	68	12.28	3.30	262	1.14	3.64	0.50
	2000	-	10	-	52	24.20	4.22	676	1.95	5.00	0.47
BIPS-A	200	0.59	3.12	6.88	72	5.72	4.86	66	1.62	5.00	0.46
	800	0.42	5.84	4.16	63	12.54	5.25	271	1.98	5.00	0.38
	2000	0.35	5.97	4.03	63	24.76	5.29	693	2.00	3.68	0.21
BIPS-B	800	0.22	7.69	2.31	63	12.43	4.88	267	1.77	5.00	0.44
BIPS-C	800	0.62	2.64	7.36	66	12.68	5.54	276	2.00	4.08	0.24
BISS-A	200	0.30	6.37	3.63	90	5.63	3.80	64	0.99	3.87	0.50
	800	0.30	7.24	2.76	65	12.43	4.85	267	1.78	5.00	0.44
	2000	0.30	6.51	3.49	63	24.72	5.27	692	2.00	3.80	0.22
BISS-B	800	0.17	8.14	1.86	63	12.42	4.82	266	1.76	5.00	0.44
BISS-C	800	0.43	4.70	5.30	66	12.54	5.42	271	1.95	5.00	0.37

4. NUMERICAL RESULTS

In order to study the nonlinear dynamic response of the BI, BIPS and BISS structures subjected to near-fault ground motions, a numerical investigation is carried out by using a step-by-step procedure (Mazza and Vulcano, 2010). At each step of the analysis, plastic conditions are checked at the potential critical sections of the girders and columns using a bilinear model with a hardening ratio of 5%. In order to take into account the plastic deformations along the girders, each of them is discretized into four sub-elements of equal length; in this way, the potential critical sections correspond to end, quarter-span and mid-span sections in Figure 3b. In the Rayleigh hypothesis, the damping matrix of the superstructure is assumed as a linear combination of the mass and stiffness matrices, assuming a viscous damping ratio of 2% in both the horizontal (ξ_H) and vertical (ξ_V) directions with reference to the two vibration periods (T_{1H} and T_{1V}) corresponding to higher-participation modes with prevailing contributions in the horizontal and vertical direction, respectively. The local damage undergone by the frame members is evaluated considering the ductility demand calculated in terms of curvature, with reference to the two loading directions, assuming as yielding curvature for the columns the one corresponding to the axial load due to the gravity loads. The response of the isolation systems is simulated using the relationships and the models described in Section 2. The ultimate values of the total shear strain ($\gamma_{tot,u}$) and the corresponding shear strain due to seismic displacement ($\gamma_{s,u}$) of a HDLRB are assumed equal to 7.5(=1.5×5) and 3(=1.5×2), respectively (i.e. 1.5 times the design values); moreover, the compressive and tensile axial loads are limited, respectively, to the critical buckling load (P_{cr}), evaluated according to the Equation 2a, and the tensile value (P_{tu}), obtained multiplying the reduced effective area by a limit stress tension σ_{tu}=0.7 MPa. The sliding friction coefficient μ_F is evaluated for mean values of contact pressure and temperature, e.g. assuming μ_{min}=3%, μ_{max}=15% and α=0.02 s/mm in the Equation 4b (see Dolce et al., 2005). According to the design hypotheses adopted for the test structures (i.e. subsoil class D and high-risk seismic region), accelerograms recorded on soft soil, with a PGA_H value approximately comparable with the one prescribed by NTC08 (PGA_H=0.404g), are considered. More specifically, near-fault ground motions recorded at Taiwan in 1999 (Chi-Chi TCU068 station: E-W and vertical components) and Imperial Valley in 1979 (El Centro D.A. station: horizontal, 360, and vertical components), available in the Pacific Earthquake Engineering Research center database (PEER, 2008), have been considered. It is interesting to note that large horizontal pulses have been observed in the Chi-Chi earthquake; on the other hand, the El Centro D.A. earthquake is characterized by a high value of the acceleration ratio α_{PGA}(=PGA_V/PGA_H).

Firstly, in order to emphasize the effects due to the horizontal and vertical components of near-fault ground motions on the inelastic response of the superstructure, the numerical investigation is carried out with reference to the BI (Figures 5a,b), BIPS-A (Figures 5c,d) and BISS-A (Figures 5e,f) base-isolation systems. To this end, mean ductility demand at all the floor levels is reported for the end-sections (Figures 5a,c,e: Chi-Chi ground motion) and mid-span sections (Figures 5b,d,f: El Centro D.A. ground motion) of the girders. For the sake of brevity, only the results for the central frame, having a tributary area for gravity loads greater than those corresponding to the lateral and interior frames (see Figure 3a), are reported for three values of the nominal stiffness ratio α_{K0}=K_{V0}/K_{H0} (i.e. 200, 800 and 2000). It should be noted that the nonlinear dynamic analyses are stopped at the time when a limit state is reached: i.e., the total shear strain of the HDLRBs or the ductility demand at the end-sections of the girders, under Chi-Chi motions; the ductility demand at the mid-span sections of the girders, under El Centro D.A. motions. Afterwards, in order to make the results comparable, the analyses have been carried out once again assuming as final instant of simulation, for each ground motion and base-isolation system, the minimum value among those before evaluated. The results obtained for Chi-Chi ground motion (Figures 5a,c,e), characterized by high values of the (horizontal) pseudo-acceleration in the range of rather long vibration periods (i.e. $T_{1H} \geq 2.5$ s), have highlighted that unexpected ductility demand are induced at the lower floors. This result is more evident for BIPS-A structures (Figure 5c), whose behaviour in the horizontal direction is that of a fixed-base structure until the friction threshold imposed by the sliding bearings is not exceeded. Moreover, it is interesting to note that, in all cases, a limited influence of α_{K0} value on the ductility demand is observed. As observed in a previous work (Mazza and Vulcano, 2012), the E-W component of Chi-Chi earthquake induces also ductility demand at the end sections of columns, especially at the lower storeys. On the other hand, under the El Centro D.A. ground motion (Figures 5b,d,f), characterized by high values of the (vertical) pseudo-acceleration at least for rather low values of the vibration periods (i.e. T_{1HV}<0.16 s), the mid-span sections of the girders undergo increasing plastic deformations for an increasing α_{K0} value, especially at the upper floors. This behaviour can be explained observing that for rather low values of α_{K0} (e.g. α_{K0}=200) the superstructure above the BI and BISS-A systems can be considered as isolated along the vertical direction, exhibiting a basically elastic

behaviour, while for rather high values of α_{K0} (e.g. α_{K0}=2000) the same superstructure can be assumed as a fixed-base structure with reference to the same direction. Moreover, a behaviour similar to that of a fixed-base structure is expected in the vertical direction for the BIPS-A systems.
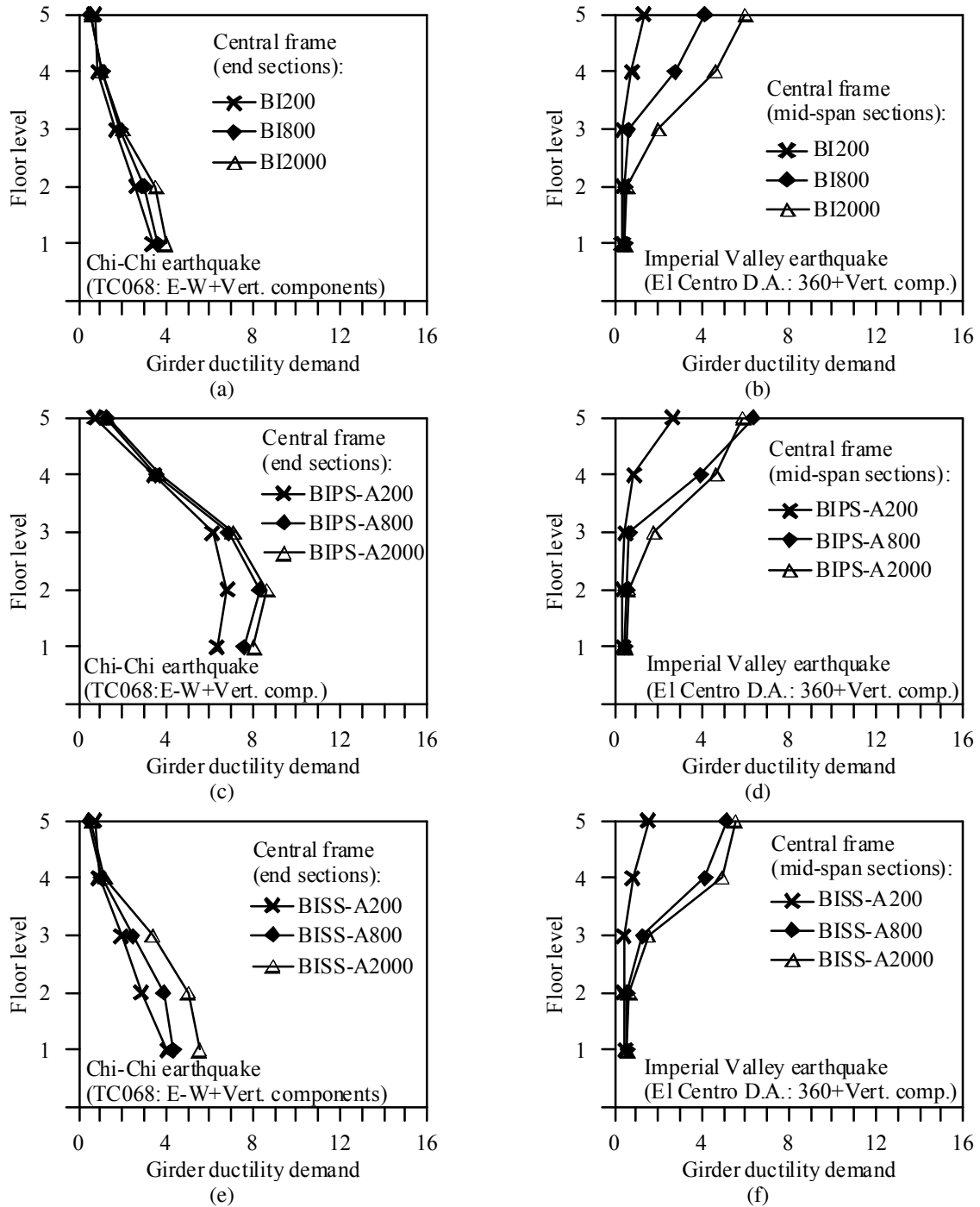

Figure 5. Effects of the nominal stiffness ratio $\alpha_{K0}(=K_{V0}/K_{H0})$ on the ductility demand of BI, BIPS and BISS structures.

Analogous curves to those shown above for the girders are reported in Figure 6 to compare the response of the BIPS and BISS base-isolation systems assuming, for a same value of α_{K0} (i.e. α_{K0}=800), three different in-plan configurations of elastomeric and sliding bearings (see Figure 4). Moreover, curves corresponding to the BI structure are also reported for a comparison. As regards the ductility demand of the end sections, the results show that for Chi-Chi ground motion (Figures 6a,c,e) both the BIPS and BISS systems have not improved the performance of the superstructure which becomes even worse of that observed for the BI structure. This is evident for increasing values of the nominal sliding ratio $\alpha_{S0}(=F_{S0}/F_{S0,max})$ when using BIPS

systems (see Table 1), because the structural behaviour in the horizontal direction tends to become ever-closer to that of a fixed-base structure. The BISS systems prove to be generally more effective than the BIPS ones for controlling the structural damage of the framed structure, producing elongation of the effective fundamental vibration period, thus limiting the maximum horizontal acceleration transmitted to the superstructure. On the other hand, ductility demand of the mid-span sections are plotted in Figure 6b,d,f for BIPS and BISS systems subjected to Imperial Valley ground motion. As can be observed, the in-plan configuration of elastomeric and sliding bearings proves of little importance, producing only moderate differences of the ductility demand at the upper floors where it is still higher than that obtained for the BI structure. Moreover, it is worth noting that the influence of α_{S0} is less evident for El Centro D.A. motion than for Chi-Chi one. The ductility demand for the columns, not shown for the sake of brevity, increases for increasing values of α_{K0}, at the top storey.
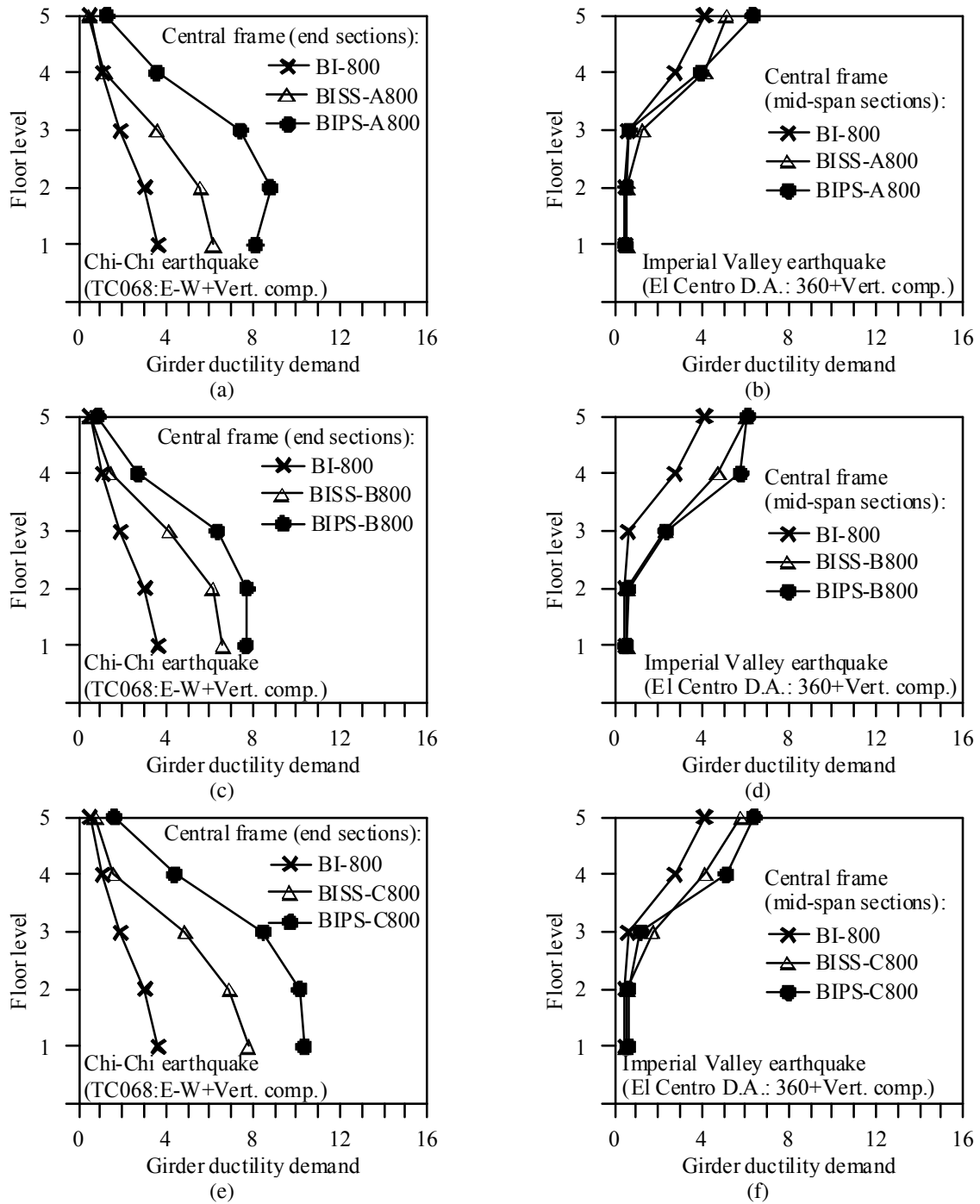

Figure 6. Effects of the nominal sliding ratio $\alpha_{S0}(=F_{S0}/F_{S0,max})$ on the ductility demand of BI, BIPS and BISS structures.

The response of the base-isolated structures is strongly affected by the behaviour of the elastomeric and sliding bearings. To this aim, the effectiveness of the BIPS and BISS systems in controlling the isolator displacement has been investigated for different values of α_{S0}. More specifically, time histories of the total shear strain (γ_{tot}) for the central isolator of the BI800, BIPS-A800 and BISS-A800 systems subjected to Chi-Chi ground motion are plotted in Figure 7a. For all cases the failure occurs before the end of motion, because the limit value $\gamma_{tot,u}$ is exceeded. In Figure 7b, analogous curves represent time histories of the horizontal displacement of elastomeric and/or sliding bearings for the exterior isolator of the central frame. As can be observed, the BIPS-A800 system is resulted the most favourable to control the isolator displacement, at least in the first 10.5 s, because the behaviour is similar to that of a fixed-base structure until the friction threshold of the sliding bearings is not reached. Residual displacement of the sliding bearings is plotted in Figure 8 for different in-plan configurations of the BIPS (Figure 8a) and BISS (Figure 8b) systems subjected to Chi-Chi ground motion. It should be noted that both systems can need re-centring after an earthquake in case the restoring force of the HDLRBs does not exceed the friction threshold of the sliding bearings. More specifically, BIPS and BISS systems undergo increasing residual displacements for increasing values of α_{S0}. Moreover, the re-centring of the BISS systems may be difficult when the residual displacement is a combination of out-of-phase movements of HDLRBs and corresponding sliding plates. Finally, histograms representing the minimum axial load (P_{min}) and the ultimate tensile axial load (P_{tu}) in the central isolator of the lateral frame are plotted in Figure 9 for BI, BIPS and BISS systems subjected to El Centro D.A. ground motion. More specifically, different values of α_{S0} are assumed for both the BIPS and BISS systems, considering a same value of α_{K0} (i.e. α_{K0}=800). As can be observed, tensile axial loads have been attained for the isolator of the BI, BIPS-A and BIPS-B structures but the P_{tu} value has never reached. Moreover, the maximum (compressive) axial load in the isolators, not shown for brevity, proves to be much less than the corresponding critical buckling load (P_{cr}).
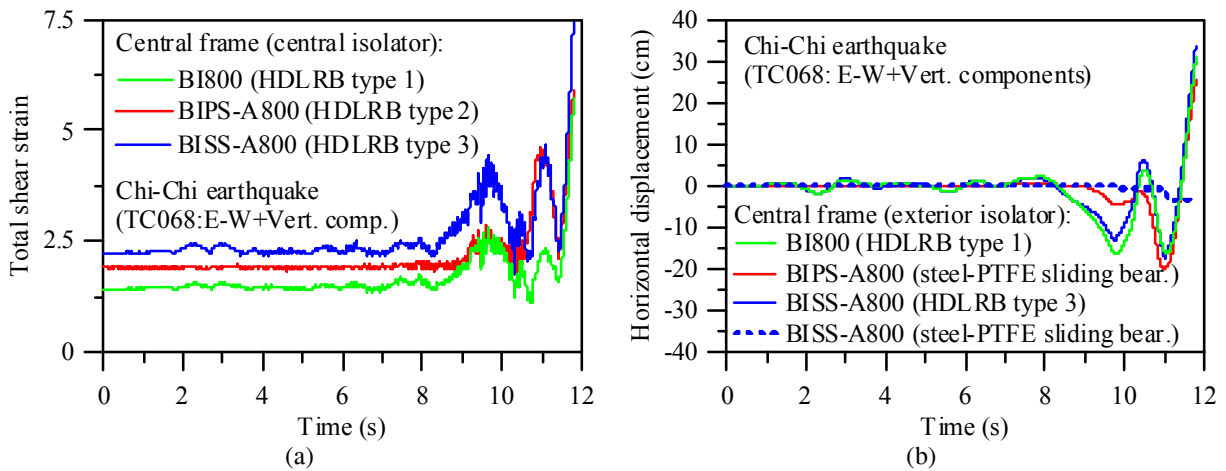

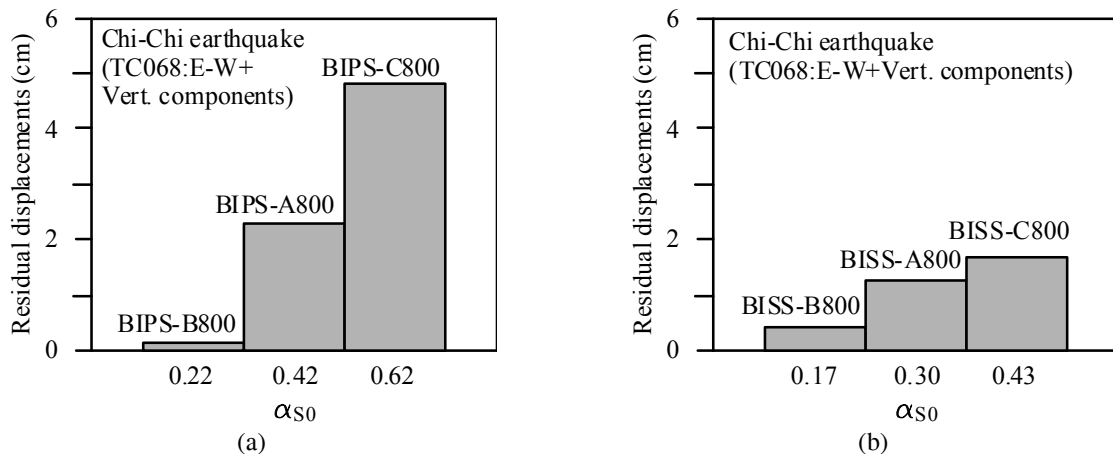**Figure 7.** Time histories for base-isolation systems of BI, BIPS and BISS structures.

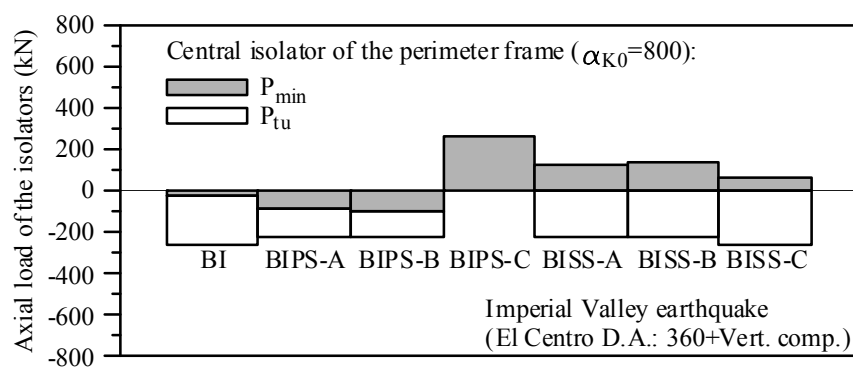**Figure 8.** Residual displacement of the sliding bearings for BIPS and BISS structures.

Figure 9. Axial load of the isolators for BI, BIPS and BISS structures.

5. CONCLUSIONS

The nonlinear seismic response of five-storey r.c. base-isolated framed structures, with different in-plan combinations and configurations of elastomeric and sliding bearings, has been studied under near-fault ground motions. Different values of the nominal stiffness ratio α_{K0}, for the HDLRBs, and nominal sliding ratio α_{S0}, for the steel-PTFE sliding plates, are considered. Under a pulse-type horizontal component of a near-fault motion, the adoption of BI, BIPS and BISS systems can induce unexpected ductility demand at the end sections of both girders and columns, especially at the lower floors. This result is more evident for increasing values of α_{S0}, especially when using a BIPS system whose behaviour in the horizontal direction tends to become ever-closer to that of a fixed-base structure. A high value of the peak vertical acceleration of the ground motion produces ductility demand rather evident at the mid-span sections of the girders, especially in the upper floors when assuming a rather high value of α_{K0} for which the superstructure behaves like a fixed-base structure in the vertical direction. The BIPS system is more effective than the BISS one for controlling the horizontal displacement of the isolation system; both systems can need re-centring after an earthquake in case the restoring force of the HDLRBs does not exceed the friction threshold of the sliding plates corresponding to the α_{S0} value. Finally, when the vertical component of the ground motion is considered, the isolators can undergo tensile loads.

REFERENCES
Braga, F., Faggella, M., Gigliotti, R., Laterza, M., (2005). Nonlinear dynamic response of HDRB and hybrid HDRB-friction sliders base isolation systems. *Bulletin of Earthquake Engineering*, **3**: 333-353.
Dolce, M., Cardone, D., Croatto, F., (2005). Frictional behaviour of steel-PTFE interfaces for seismic isolation. *Bulletin of Earthquake Engineering*, **3**: 75-99.
Kasalanati, A., Constantinou, M.C., (2005). Testing and modeling of prestressed isolators. *Journal of Structural Engineering*, **131**: 857-866.
Kelly, J.M., (2003). Tension buckling in multilayer elastomeric bearings, *J. of Engrg. Mechanics*, **129**: 1363-1368.
Mazza, F., Vulcano, A., (2009). Nonlinear response of rc framed buildings with isolation and supplemental damping at the base subjected to near-fault earthquakes, *Journal of Earthquake Engineering*, **13**(5): 690-715.
Mazza, F., Vulcano, A., (2010). Comparison among base isolation techniques for r.c. buildings subjected to near-fault earthquakes. *14th European Conf. on Earthquake Engineering*, Skopije, Republic of Macedonia, paper No. 337.
Mazza, F., Vulcano, A., (2012). Effects of near-fault ground motions on the nonlinear dynamic response of base-isolated r.c. framed buildings. *Earthquake Engineering and Structural Dynamics*, **41**: 211-232.
Naeim, F., Kelly, J.M., (1999). Design of seismic isolated structures: from theory to practice, *Wiley & Sons Ltd, NY*.
Pacific Earthquake Engineering Research center, (2008). Next Generation Attenuation (NGA) database. *http://peer.berkeley.edu/peer_ground_motion_database*
Ryan, K.L., Chopra, A.K., (2006). Estimating seismic demands for isolation bearings with building overturning effects. *Journal of Structural Engineering*, **132**: 1118-1128.
Ryan, K.L., Kelly, J.K., Chopra, A.K., (2004). Experimental observation of axial load effects in isolation bearings, *Procs. of the 13th World Conference on Earthquake Engineering*, Vancouver (Canada), paper No. 1707.
Technical Regulations for the Constructions. Italian Ministry of the Infrastructures, January 14, 2008 (in italian).